JOURNAL OF GEOPHYSICAL RESEARCH, VOL. 89, NO. D4, PAGES 5345-5353, JUNE 30, 1984

Sample Size and Scene Identification (Cloud): Effect on Albedo

SASTRI K. VEMURY[1]

Research and Data Systems, Inc.

LARRY STOWE AND HERBERT JACOBOWITZ

NOAA/National Environmental Satellite Data Information Service

Scan channels on the NIMBUS 7 Earth Radiation Budget (ERB) instrument sample radiances from underlying earth scenes at a number of incident and scattering angles. A sampling excess toward measurements at large satellite zenith angles is noted. Also, at large satellite zenith angles, the present scheme for scene selection is causing many observations to be classified as cloud, resulting in higher flux averages. Thus, the combined effect of sampling bias and scene identification errors is to overestimate the computed albedo. It is shown, using a process of successive thresholding, that observations with satellite zenith angles greater than 50°–60° lead to incorrect cloud identification. Elimination of these observations has reduced the albedo from 32.2 to 28.8%. This reduction is very nearly the same and in the right direction as the discrepancy between the albedoes derived from the scanner and the wide field-of-view (WFOV) channels.

1. INTRODUCTION

Estimates of the earth radiation budget have been made for more than a decade, using observed radiances from orbiting satellites. Several authors [*Vonder Haar and Suomi*, 1971; *Ellis and Vonder Haar*, 1976; *Gruber and Winston*, 1978; *Jacobowitz et al.*, 1979; *Stephens et al.*, 1981; *Jacobowitz et al.*, this issue] have obtained the radiation budget parameters either from most recent available data or from accumulated data sets extending to 1964. *Stephens et al.* [1981] provide a discussion on some of the assumptions made in these studies, the limitations caused by instrumental resolution, varying spatial and temporal coverages, and uncertainties in the determination of flux densities at the top of the atmosphere from radiance measurements at the satellite. Confidence in the final estimates would critically depend on the reliability of the estimation methods of the budget parameters. Of the three parameters that enter into the equation, the most uncertain quantity by present understanding is the amount of reflected shortwave radiation or the corresponding planetary albedo. This parameter (on a spatial scale of interest to climate and atmospheric modelers) is sensitive to the underlying earth surface (including clouds) and to the sun-satellite configuration with respect to the viewed point. The latter of the two, viz., correction of the radiance measurements for scattering geometry and solar elevation angle can be performed adequately by application of models for the underlying scene. Such models have been developed by *Ruff et al.* [1968], *Raschke et al.* [1973], among others and more recently by *Stowe et al.* [1980] and *Taylor and Stowe* [this issue]. Determination of the underlying surface, particularly presence of cloud, continues to be a problem, and part of the investigations in the present paper will deal with the systematic biases, in the estimation of reflected fluxes, caused by incorrect scene identification.

Also of interest for all satellite-derived measurements is the averaging procedure used in arriving at a mean value for the albedo at the top of the earth/atmosphere system for an area nearly 500 × 500 km on the earth's surface. During the period of transit, the satellite instruments view any location several times. Each radiance observation is converted into an estimate of the mean daily reflected flux through adjustments which depend on surface type and geometry. Several observations then provide a mean value for the day. The question being addressed is whether these observations should be treated equally or should be weighted according to the time of observation or according to the viewing angles.

Of the 22 channels on the Earth Radiation Budget (ERB) instrument, 8 are scanning channels (15–22) with a narrow field of view (NFOV) which measure the incoming radiance from different earth scenes over a wide variety of incident and viewing angle configurations. Channels 15–18 observe the broadband SW reflected solar radiation, while channels 19–22 measure the broadband outgoing longwave radiation. The scanner can operate in five different scan modes, four of which provide an extensive range of angular views of a target on the earth, while the fifth is a composite of the scan modes 3 and 4 applied in that order [*Jacobowitz et al.*, 1978]. The scan patterns for modes 1–4 are repeated every 112 s. The observations in these modes provide extensive coverage in the principal plane of the sun. Scan mode 5 is repeated every 224 s and is capable of providing maximum coverage of the earth. These modes can be altered to change the angular extent of coverage from one to the other on command.

Albedoes obtained by using the scan channel radiances (referred to as NFOV albedoes) were shown to be larger than the corresponding albedoes determined from the wide field of view (WFOV) channels on the instrument (*Jacobowitz et al.* [this issue], for monthly averages). The present study demonstrates the existence of biases in processing the NFOV reflected radiances and offers alternative schemes to improve global estimates of the albedo.

The NFOV shortwave channels 15–18 were stable except for channel 18, which was found to be erratic after December 27, 1978. The sensitivity of the channels is reported to vary by less than 1%, though they are about 5–15% different

[1] Now at S M Systems and Research Corp.

Paper number 3D1853.

TABLE 1. Sampling Scheme for Radiance Measurements With the Scanner at Different Nadir Angle Ranges During an Outward Scan to the Horizon

Step	Number of IFOVs Integrated Per Observation*	Angular Extent of Each Observation	Number of Observations in the Range	Nadir Angle Range	Cumulative Total of Number of Observations
1	20	5°	7	0°–35°	7
2	10	2.5°	6	35°–50°	13
3	4	1.0°	6	50°–56°	19
4	1	0.25°	19	56°–60.75°	38

*Each IFOV consists of radiant energy received through an instantaneous field of view of 0.25° × 5.12°.

from the pre-flight calibration sensitivity. This was determined from in-flight tests performed (1) by using solar illuminated diffuse check target results, (2) through wide/narrow intercomparisons using the wide field of view channels (channels 11–14), and (3) through observations of cloud free snow/ice surfaces for which ground-based observations exist. It is obvious from the tests that the shortwave scan channels aboard the instrument have performed quite satisfactorily during the period of their operation except for channel 18. Data after December 27, 1978, for channel 18 are ignored.

Scanner data from different days, which are nearly 6 months apart, have been utilized in this paper to evaluate the population (sample size) differences, associated biases in the computed fluxes, and preferences in scene selection. Some simple schemes to eliminate or reduce the sampling and flux biases are outlined. Results obtained with these schemes are presented in view of their impact on the computed products. Conclusions and some suggestions for improving the present scene selection scheme are outlined including a discussion of methods to eliminate or reduce the existing biases in averaging.

2. Sampling Biases Due to Scan Steps

The five modes, mentioned before, consist of scans in the orbital plane parallel to the direction of the velocity vector and in a plane perpendicular to the same. In the orbital plane, the scanning is performed up to the horizon, while in the plane perpendicular to the orbital plane, the scan is out to a nadir angle of 56°. These are referred to as the long grid and short grid, respectively [see *Jacobowitz et al.*, 1978]. The scanning proceeds from nadir to the horizon, the gimbal is turned 6° at the horizon, and an inward scan begins [see *Jacobowitz et al.*, this issue, Figure 6]. This is intended to provide a better spatial coverage of the underlying surface. The same process is repeated with the short grid except that the outward scanning is terminated at 56° in nadir angle.

A certain amount of radiant energy is received by the scanner during an instantaneous field of view (IFOV) of the earth scene. One or more of these IFOV energies are integrated to obtain one radiance measurement or one observation. Several such observations constitute one scan step. When the scan step is altered, the number of IFOV's for each measurement and the number of such measurements

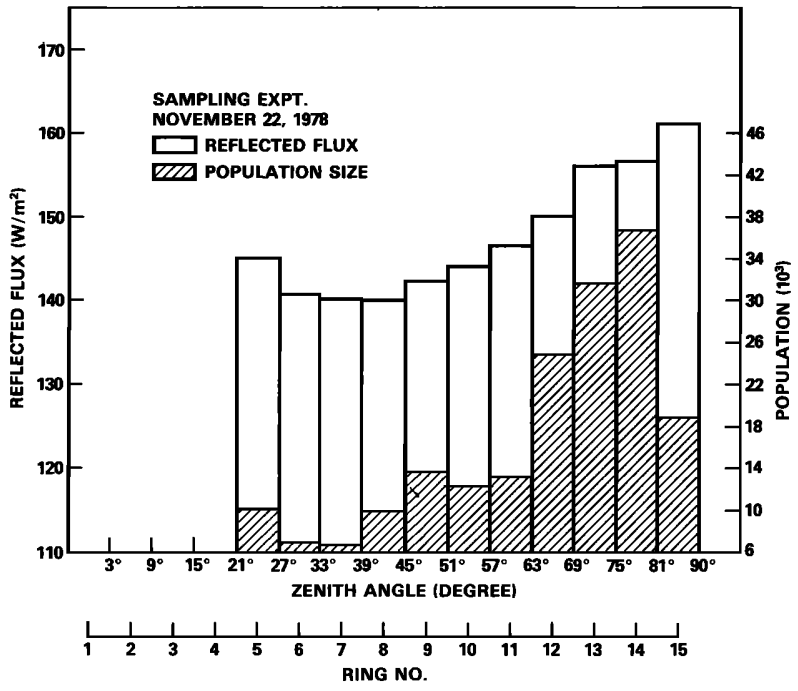

Fig. 1. Averaged reflected fluxes (W/m²) and population size (in thousands) for 15 satellite zenith angle intervals. The intervals are also shown in degrees. Data for November 22, 1978.

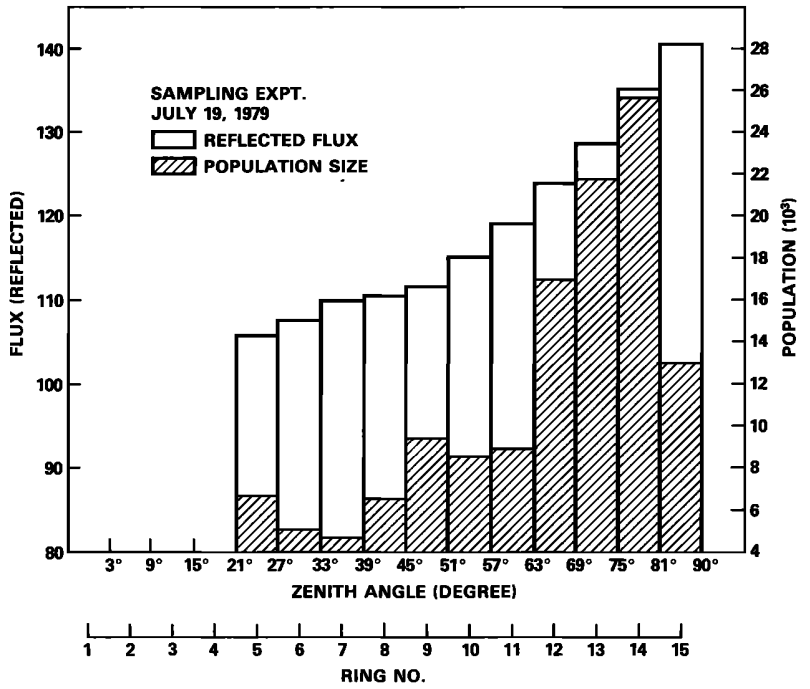

Fig. 2. Same as in Figure 1. Data for July 19, 1979.

also change. The different parameters in the scanning procedure are shown in Table 1. For example, in scan step 1, there are seven observations made, each consisting of an angular extent (in nadir angle) of 5° for a total of 35°. Each of these 5° observations consists of integration over radiant energies during 20 IFOV's, 0.25° each in nadir angle. The scan step is then altered to obtain six observations of angular extent, 2.5° each which in turn are integrated energies over 10 IFOV's of 0.25° in nadir angle.

This procedure is continued as shown in Table 1 until the horizon is viewed at nadir angle of 60.75°. Each of these individual measurements consists of radiant energy received from a ground resolution of nearly 150 km. Thus, from Table 1, there are 19 observations during scan steps 1–3 ranging from 0° to 56° in nadir angle (56° nadir angle corresponds to a satellite zenith angle of nearly 72° for NIMBUS 7 orbit). In the nadir angle range 56°–60.75° (corresponding to 72°–90° in satellite zenith angle), there are also 19 observations. Thus half the number of observations are for satellite zenith angles greater than 72° approximately. Thus in a sampling scheme where each measurement receives equal weight, the observations in the zenith angle range 72°–90° receive greater weight, simply due to their large numbers.

The actual population sizes for a given day at different satellite zenith angles are shown in Figures 1 and 2. The cross-hatched portions correspond to population sizes in both figures and the scale is shown on the right. Figure 1 is for observations from November 22, 1978, scanner data, and Figure 2 is the same for July 19, 1979. The populations are determined for each of 15 satellite zenith angle rings consisting of an inner ring of 3°, 13 concentric rings of 6° each, and one outer ring (15th) of 9°. These ring numbers are indicated on the figure. It is apparent from the figures that the three or four outer rings combined have nearly twice as much population as all the inner rings put together. Observations in the inner most rings (satellite zenith angles 0°–21°) have been ignored in the present study. This is done to avoid the incorrect scene selection using the IR and visual radiance measurements at these angles. Details about the bispectral scheme for scene selection will be discussed in section 4.

TABLE 2. Percentages of Cloud and Noncloud Classifications for Satellite Zenith Angles Less Than and Greater Than 70°

TA	Date of Observations	Total Number of Observations	Number of Observations With Sat Zen >70°*		Number of Observations With Sat Zen ≤70°*		Percent Cloud Classification (Sat Zen >70°)*	Percent Cloud Classification (Sat Zen ≤70°)*
			Cloud	Noncloud	Cloud	Noncloud		
1070	Nov. 22, 1978	159	104		55		18%	0%
(2.25N, −155.25W)			19	85	0	55		
1043	Nov. 22, 1978	125	40		85		85%	55%
(2.25N, −33.75W)			34	6	47	38		
1096	June 22, 1979	60	19		41		66%	16%
(2.25N, 87.75E)			13	6	7	34		
1417	June 22, 1979	49	22		27		88%	11%
(20.5N, 47.25E)			19	3	3	24		

*Sat Zen refers to satellite zenith.

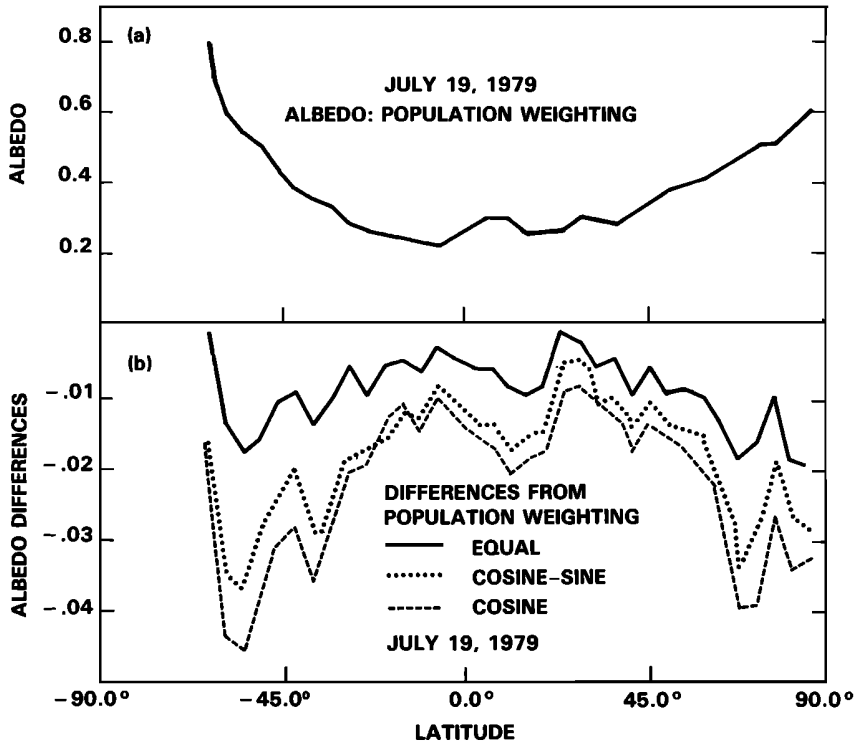

Fig. 3. (*a*) Zonally averaged albedoes for July 19, 1979, with population weighting; (*b*) albedo differences for different weighting schemes from population weighting.

3. Biases in Computed Fluxes

Each radiance observation is converted to a mean daily albedo by the application of models (1) to correct for anisotropy of reflection and (2) to account for variation of the reflectance of the identified surface during the period from sunrise to sunset. The first factor, viz., the anisotropy of reflection, is a function of satellite zenith and relative (to the sun) azimuth angles for a given underlying surface and a solar zenith angle. These models are the bidirectional reflectance models usually referred to as angular distribution models (ADM) and are discussed in detail in *Taylor and Stowe* [this issue].

The second factor is a function of the solar zenith angle and is necessary to convert the instantaneous reflectance to a mean daily albedo. This factor is supplied by another model which represents the variation of reflectance with solar zenith angle [see *Raschke et al.*, 1973, Figure 1]. This set of models (which may be considered to represent diurnal variation) is called the directional model.

Mean daily reflected fluxes from all radiance measurements for a given day are sorted into 15 satellite zenith angle rings, as previously noted. The flux averages for each of the rings are shown in Figure 1 for data on November 22, 1978, and in Figure 2 for July 19, 1979. The reflected fluxes are shown as histograms for each of the rings and the scale (in W/m^2) is shown on the left.

It is apparent from these figures that the reflected flux averages are nearly the same for the inner rings and tend to become large by nearly 15–20% for the three or four outer rings corresponding to satellite zenith angles 69° and above. We first note that, a priori, there is no reason to expect widely different flux estimates for different zenith angle rings. There apparently is a bias in the flux estimation. In any case, the effect of higher flux averages for the outer rings is to overestimate the total averaged reflected flux and thus the albedo. This effect is amplified by the large population sizes (discussed in the previous section) associated with these angles. We must also mention that the differences in populations themselves would not have any effect if there are no biases in the flux averages for the rings. The nature of these biases is the subject of the next section.

4. Problems With Scene Identification

Simultaneous measurements of the reflected and emitted radiance, N_R and N_E from the scene, are used to identify the underlying scene. Instead of N_R the quantity that is generally used is $\pi\rho$ defined by

$$\pi\rho = \frac{\pi N_R}{S_0\, L(t) \cos \zeta} \tag{1}$$

where S_0 is the solar constant at 1 A.U. and $L(t)$ is the reciprocal of the normalized earth sun distance square and ζ is the solar zenith angle at the time of reflected radiance measurement. Knowing $\pi\rho$ and emitted radiance N_E, the scene is determined as follows: for latitudes greater than 67.5°N or S, snow, $\pi\rho > 0.5$; cloud, $0.15 < \pi\rho \leq 0.5$; ocean, $\pi\rho \leq 0.15$; and for latitudes less than 67.5°, ocean, $\pi\rho \leq 0.15$; land, $\pi\rho > 0.15$ and $N_E > 78.2\ \mathrm{Wm^{-2}\ sr^{-1}}$; cloud, $\pi\rho > 0.15$ and $N_E \leq 78.2\ \mathrm{Wm^{-2}\ sr^{-1}}$.

This scheme was used by *Saunders et al.* [1983] in their comparisons of radiation budget estimates from different satellites. In the vicinity of the specular point, the scheme leads to incorrect identification and thus all observations which are within 21° in satellite zenith and 30° on either side of the 180° relative azimuth are excluded from processing [*Saunders et al.*, 1983]. The angular models used in the

TABLE 3. Globally Averaged Albedoes for Data for November 22, 1978, and July 19, 1979

Sampling Scheme	Albedoes			
	Nov. 22, 1978		July 19, 1979	
	Mean	Standard Deviation	Mean	Standard Deviation
Population weighting	0.347	0.130	0.312	0.075
Equal zone weighting	0.342	0.130	0.305	0.073
Cosine weighting	0.334	0.130	0.294	0.070
Cosine-sine weighting	0.336	0.130	0.297	0.071

present study, however, are improved models compared to the ones used by them. The lack of observations in the satellite zenith angle range 0°–21° noted in section 2 is a direct result of the exclusion of these radiances.

Once a scene is identified from the two simultaneous SW and LW radiance measurements form the viewed region, a reflected flux is then computed by applying the appropriate bidirectional reflectance model and the directional model. It is known that the bidirectional reflectances for outgoing flux densities are critically dependent upon the type of underlying earth surface or cloud [*Arking and Levine*, 1967; *Ruff et al.*, 1968; *Raschke et al.*, 1973; *Taylor and Stowe*, this issue]. Surfaces like cloud and snow/ice have higher albedo than ocean, but tend to be less anisotropic. An incorrect scene identification could thus lead to an error in the flux computed from a radiance observation.

Correct cloud detection, generally, is a problem. In the processing of SW scan channel data and in the present study, cloud is mostly identified by using a threshold on the observed longwave radiance and over snow-covered regions, using thresholds on the instantaneous albedo. These thresholds are constants and are not sensitive to either the satellite zenith angle or to the underlying earth surface. To evaluate the adequacy of the scene selection scheme statistics on cloud selection were collected for a complete day, for four target areas (TA) at two times of the year, viz., November 22, 1978, and June 22, 1979. The results are presented in Table 2. For each TA, the total number of observations during the day is broken down into the number of observations with satellite zenith angles greater than and less than or equal to 70°. The number and percentage of cloud and noncloud classifications under each category for each TA are shown in the table. For TA 1070 (with center at latitude = 2.25°N, longitude = 155.25°W) there were 104 observations. For satellite zenith angles greater than 70°, 18% of these received cloud classifications. At satellite zenith angles less than 70°, none or 0% were classified as cloud on June 22, 1979. For TA 1417 (latitude = 20.5°N, longitude = 47.25°E), 88% of the observations at satellite zenith angle greater than 70° were classified as cloud, while only 11% were considered cloud at angles less than 70°. It is, thus, apparent that the present identification scheme is selecting cloud preferentially at large satellite zenith angles. Clouds, in general, are less anisotropic than other surfaces identified in the scheme and tend to have a large bidirectional reflectance factor, particularly at large satellite zenith angles. Ocean, on the other hand, is highly anisotropic, and, for the same satellite zenith angle, the reflectance factor is smaller compared to the cloud case. For a given radiance measurement at that satellite zenith angle, a cloud identification would thus lead to a higher estimate of the reflected flux.

5. Elimination of Biases

The sample size, noted earlier, is intrinsically not a problem. But, when associated with flux biases in the same sense as the population biases, the situation becomes worse and needs to be corrected. Four different weighting schemes are applied to the data to evaluate the impact on the final albedo. The fluxes are averaged for each of the 15 satellite zenith angle rings, and these fluxes F_i are weighted differently in each case. To reduce the effect of the sample size, the 15 ring means are weighted equally. To account for the enhanced fluxes at large satellite zenith angles, a cosine weighting is used. Since irradiance measurement by WFOV channels tends to integrate the radiances I in the form

$$F = \int_{\theta=0}^{\pi/2} \int_{\phi=0}^{2\pi} I(\theta, \phi) \cos\theta \sin\theta \, d\theta \, d\phi \qquad (2)$$

(where $I(\theta, \phi)$ is the radiance measured at satellite zenith and azimuth angles θ and ϕ, respectively), a cosine-sine weighting scheme is also employed. Finally, the effect of complete elimination of all observations at satellite zenith angle greater than 70° is also studied.

The first method gives the average flux in each of the 15 satellite zenith angle rings (discussed before) an equal weight. Thus, the effect of the larger population in the outer rings is eliminated. This method is referred to as the "equal averaging" method, and the averaged reflected flux is denoted by F_E. Denoting the mean flux for each of the 15 satellite zenith rings by F_i and the respective population by N_i, this weighting is equivalent to computing

$$F_E = \sum_{i=1}^{15} F_i W_i \Big/ \sum_{i=1}^{15} W_i \qquad (3)$$

TABLE 4. Global Cloud Cover Estimates

Date	Number of Observations					
	All Satellite Zenith Angles			Eliminate Observartions With Zenith Angle > 70°		
	Total Number	Cloud Number	Cloud Percent	Total Number	Cloud Number	Cloud Percent
Nov. 22, 1978	201,393	109,675	54.56	112,757	53,132	47.12
June 22, 1979	134,631	71,096	52.81	74,931	33,673	44.94
Oct. 14, 1979	132,100	74,224	56.19	73,025	35,246	48.27

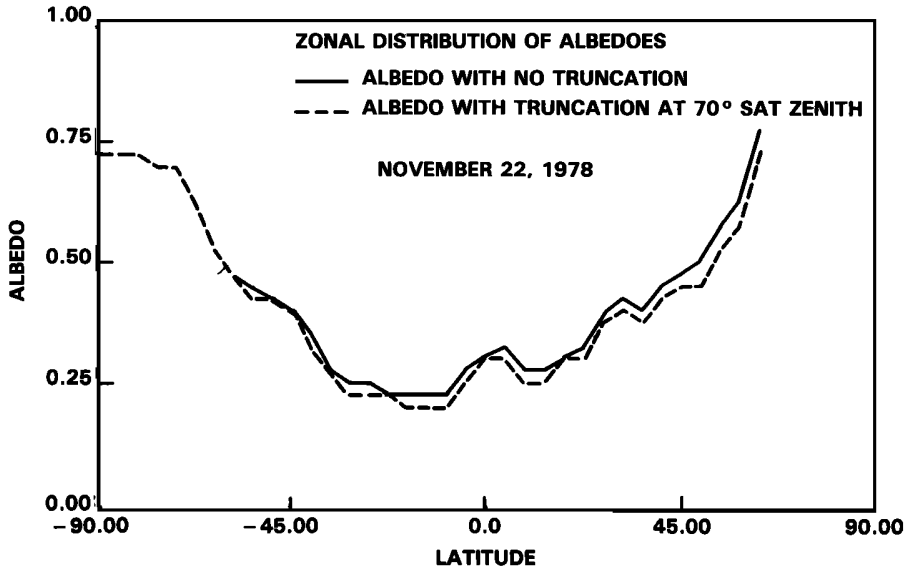

Fig. 4. Zonal distribution of albedoes for November 22, 1978. The dash line shows the results with truncation at 70° in satellite zenith angle.

where

$$W_i = 1 \quad \text{if} \quad N_i > 0$$
$$W_i = 0 \quad \text{if} \quad N_i = 0.$$

Since it has been determined that the problem is with the reflected fluxes at large satellite zenith angles, a smooth function that reduces the effect of inaccurate flux values at those angles, namely, cosine of satellite zenith angle, may be used for weighting. This will be referred to as "cosine weighting" method and the flux, F_C, will be computed according to

$$F_C = \sum_{i=1}^{15} W_i F_i \Big/ \sum_{i=1}^{15} W_i \tag{4}$$

with

$$W_i = \cos \theta_i \quad \text{if} \quad N_i > 0$$
$$W_i = 0 \quad \text{if} \quad N_i = 0$$

where θ_i is the mean satellite zenith angle of the ring.

For purposes of comparison with the wide field of view (WFOV) channels on the ERB instrument, an averaging

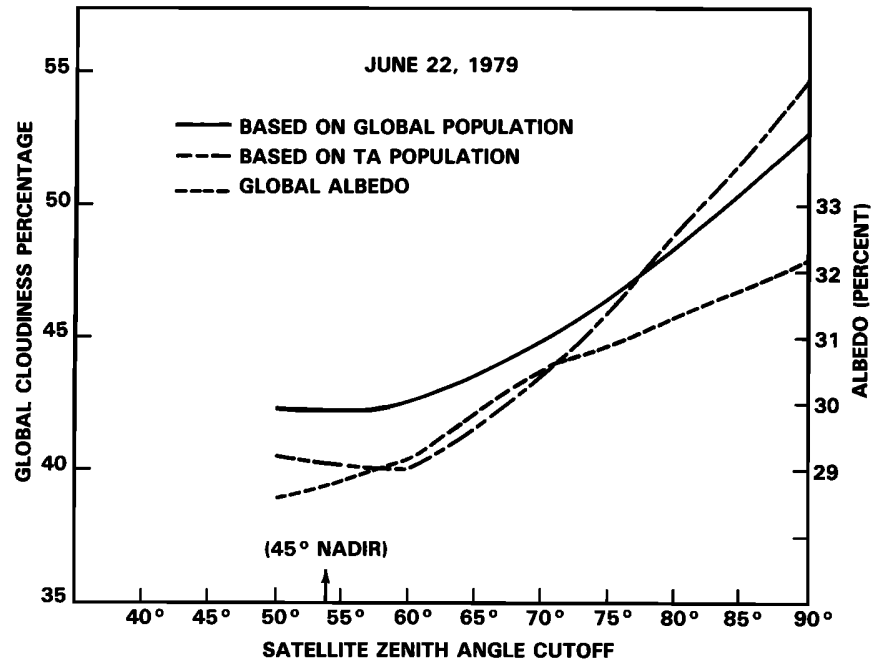

Fig. 5. Effect of truncating observations at different satellite zenith angles on the global cloud cover and the global albedo. The truncation level used (45° nadir) by *Raschke et al.* [1973] for NIMBUS 3 observations is indicated by an arrow.

scheme which utilizes the "cosine-sine weighting" of the zenith ring mean fluxes is employed. The wide angle instruments tend to give much smaller weight to observations near the nadir and the limb (equation (2)). The computed average will be denoted by F_{CS}, given by

$$F_{CS} = \sum_{i=1}^{15} W_i F_i \Big/ \sum_{i=1}^{15} W_i \tag{5}$$

with

$$W_i = \cos\theta_i \sin\theta_i \quad \text{if} \quad N_i > 0$$

$$W_i = 0 \quad \text{if} \quad N_i = 0$$

The scheme, currently employed in the routine processing of the NFOV radiances, gives equal weight to all observations and may be called the "population weighting." This is equivalent to

$$F_{pop} = \sum_{i=1}^{15} W_i F_i \Big/ \sum_{i=1}^{15} W_i \tag{6}$$

with

$$W_i = N_i \quad \text{if} \quad N_i > 0$$

$$W_i = 0 \quad \text{if} \quad N_i = 0$$

where N_i is the sample size for the ith ring.

The existence of a problem with scene identification was noted in the previous section, particularly at large satellite zenith angles. This problem may be avoided by rejecting all observations at those angles, particularly at angles greater than 70°. We note that in processing NIMBUS 3 data, all observations at nadir angles greater than 45° [*Raschke et al.*, 1973] were rejected in a similar manner to avoid errors due to "shielding by heterogeneous clouds." This method which eliminates observations at large satellite angles will be referred to as "population weighting with truncation."

The above procedures have been applied to the NFOV radiance data from November 22, 1978, and July 19, 1979. The effect on the zonally averaged and global albedoes are discussed below.

6. Results

The zonal averages of the albedo for different weighting schemes are plotted in Figure 3 from the data for July 19, 1979. The results are qualitatively similar for November 22, 1978. From this plot, it is apparent that the "equal weighting" scheme reduces the zonal averages only slightly. The cosine and cosine-sine weighting methods reduce the zonal averages for most of the equatorial and midlatitude regions. Near the terminator, the differences in the schemes are not significant.

Globally averaged albedoes with standard deviations are shown in Table 3. The population weighted (normal) global mean albedo for November 22 is 0.347, while the cosine weighting method gives a value of 0.334. This globally averaged albedo is reduced by 0.013 or 4% by reducing the weight given to the averages from the outer satellite zenith angle ring. The equal weighting method has the effect of eliminating only the population biases while retaining the flux biases. The global average albedo in this case is changed only by 0.005 or 1.5%. The real problem as we noted earlier is not the population size but the large fluxes produced by incorrect scene identification. Albedo changes of similar magnitude from the data for July 19, 1979, are also shown in the table. In both cases it is apparent that the removal of population bias has a much smaller effect on the global mean albedo as compared to the near elimination of the effect of large satellite angles.

TABLE 5. Effect of Satellite Zenith Angle Truncation on the Computed Global Albedo

Date	Truncation Level		
	90°	70°	50°
Nov. 22, 1978	0.347	0.331	0.315
June 22, 1979	0.322	0.305	0.288
July 19, 1979	0.312	0.294	0.281

In view of the difficulty with scene identification at large satellite zenith angles discussed in section 4, a separate experiment was conducted in which all observations at satellite zenith angles greater than 70° were eliminated. This truncation is found to reduce the global albedo by 0.016, viz., from 0.347 to 0.331 for November 22, 1978. The zonal averages of the albedo for this case are shown in Figure 4 by the dashed line, while the solid line denotes the albedo with all observations. The albedo with truncation is smaller in all cases except in the region near the south pole. At latitudes south of 67.5°, no difference is expected since emittance threshold is not used at these latitudes. The implication is that truncation, as expected, is generally eliminating large flux contributions which would come from inaccurate scene selection.

The truncation also has the effect of reducing the number of TAs observed on this day, from 1626 TAs to 1568. These 58 TAs apparently have all observations at satellite zenith angles greater than 70°. The albedo obtained after truncation for the 1568 TAs are compared with the albedo when no truncation was in effect. A regression analysis of the TA albedoes with and without truncation (Y and X, respectively) has led to the relation

$$Y = -0.018 + 1.003\,X$$

7. Estimates of Global Albedo

The results of the previous section provide a scheme for elimination of the problem associated with scene selection. It is clearly shown that the effect of ignoring observations at satellite zenith angles greater than 70° (or nadir angles greater than 55°) is to reduce the global albedo estimate. Associated with this is the decrease in global cloud cover estimate. Results in Table 4 indicate that elimination of observations with satellite zenith angle greater than 70° decreased the cloud cover by nearly 7%. The results are consistently the same on the three days studied, viz., November 22, 1978, June 22 and October 14, 1979.

The above cloudiness estimates were derived simply from the total cloud classifications relative to the number of total observations on any given day. This is referred to as cloudiness (global population based). To avoid sample size differences among different target areas due to orbital characteristics, another global cloudiness estimate which de-

pends upon the number of cloud classifications in a TA is also derived. This is referred to as the cloudiness (TA population based). The satellite zenith angle threshold is successively decreased, and the corresponding cloudiness estimates are determined with both the methods. The results for June 22, 1979, are shown in Figure 5, with the threshold value of the zenith angle on the abscissa and the global cloudiness estimate as the ordinate. Both the cloudiness estimates, viz., based upon the global populations and upon the TA populations, tend to level off in the 50°–60° satellite zenith angle range. Also shown is the threshold (45° nadir angle) used by *Raschke et al.* [1973] in processing NIMBUS 3 MRIR observations. It lies in the range (50°–60° satellite zenith angle) that is established with the present study.

Global cloudiness estimates per se are not the subject of this paper. They only provide an insight into the satellite zenith angle range for which the cloud classification may not be reliable. Of interest is the estimate of global albedo. The albedo curve is also shown in Figure 5 with the scale on the right. The albedo decreases from 0.322 to nearly 0.290 if observations with reliable scene identification only are utilized. This is particularly significant in view of the results presented by *Jacobowitz et al.* [this issue]. The NFOV monthly averaged albedoes are consistently larger by nearly 0.03 than the WFOV monthly averages. The effect of truncation on the global albedo is presented in Table 5 for three days, viz., November 22, 1978, June 22 and July 19, 1979, for truncation at 70° and 55°. In all cases, the global albedo is reduced, at the 55° truncation level, by 0.03 which is nearly the same as the present NFOV, WFOV albedo difference.

8. Conclusions and Prognosis

Data from scanning channels on the NIMBUS 7 ERB instruments have been used in this investigation to evaluate the effect of sample size and of improving scene identification (cloud in particular) on the computed albedoes. It is shown that the stepping pattern in the scanning procedure causes differences in sample size at large and small satellite zenith angles. A problem with the scene identification that has been noted from observations is that a cloud scene is being selected more frequently at large satellite zenith angles. This, coupled with the larger population sizes due to scan pattern in the same satellite zenith angle ranges, has caused an overestimation of the computed albedo when all observations are equally weighted. The effect of differences in sample size is removed by determining mean zenith ring fluxes which then are averaged to obtain the mean flux. This has decreased the albedo by about 1.2% compared to the previous result. This implies that the sample size plays a minor role. Two other schemes which reduce the weight for observations at large satellite zenith angles (cosine weighting, cosine-sine weighting), have been found to reduce the albedo by nearly 5%.

The problem with scene identification seems to be elimated if all observations with satellite zenith angle greater than 55° are eliminated. The uncertain cloud classifications associated with large satellite zenith angles are thereby removed and the cloudiness estimates level off to an asymptotic value in the 50°–60° zenith angle range. The albedo corresponding to that situation may be considered to be an "unbiased" estimate of the global albedo, in the sense that the biases due to scene identification are removed. The associated decrease in the albedo is about 0.03 which also is the albedo difference between the NFOV and WFOV albedoes.

Some alternatives to an accurate computation of global albedoes relate to improved scene selection particularly for cloud. They consist of the following points:

1. Utilization of near simultaneous cloud information available from the THIR instrument. The sub-target radiance (STR) data base [*Stowe and Fromm*, 1983] contains the scene identification information along with the radiance data from ERB scanners. This scene and cloud information may be more reliable than the thresholding methods employed in processing the data.

2. Scene selection from reflected and emitted radiance measurements may be improved by using computed radiance means and standard deviations through some established statistical techniques.

3. Development of averaging schemes which will eliminate biases due to sample size and to scene identification errors.

Acknowledgments. We are grateful to H. Lee Kyle of NASA, Goddard Space Flight Center and George Ohring of NOAA/NESDIS for valuable and informative discussions on this work. We would also like to thank R. Shah for aiding in some of the computations reported here. One of us (S. K. V.) is pleased to acknowledge support from NASA/GSFC under contract NAS5-26123.

References

Arking, A., and J. S. Levine, Earth albedo measurements: July 1963 to June 1964, *J. Atmos. Sci., 24*,721–724, 1967.

Campbell, G. G., and T. H. Vonder Haar, Climatology of radiation budget measurements from satellites. *Atmos. Sci. Pap. 322*, Colo. State Univ., Fort Collins, Colo., 1980.

Ellis J. S., and T. H. Vonder Harr, Zonal average earth radiation budget measurements from satellites for climate studies, *Atmos. Sci. Pap. 240*, Colo. State Univ., Fort Collins, Colo., 1976.

Gruber, A., and J. S. Winston, Earth atmosphere radiative heating based on NOAA scanning radiometer measurements, *Bull. Am. Meteorol. Soc., 59*, 1570–1573, 1978.

Jacobowitz, H., L. L. Stowe, and J. Hickey, The NUMBUS-7 Users' Guide, pp. 33–69, NASA, 1978.

Jacobowitz, H., W. L. Smith, H. B. Howell, and F. W. Nagle, The first 18 months of planetary radiation budget measurements from the NIMBUS-6 ERB experiment, *J. Atmos. Sci., 36*, 501–507, 1979.

Jacobowitz, H., R. J. Tighe, and the NIMBUS 7 Experiment Team, The earth radition budget derived from the NIMBUS 7 ERB experiment, *J. Geophys. Res.*, this issue.

Raschke, E., T. H. Vonder Haar, W. R. Bandeen, and M. Pasternak, The annual radiation balance of the earth-atmosphere system during 1969–70 from NIMBUS-3 measurements, *J. Atmos. Sci., 30*, 341–364, 1973.

Ruff, I., R. Koffler, S. Fritz, J. S. Winston, and P. K. Rao, Angular distribution of solar radiation reflected from cloud as determined from TIROS IV radiometer measurements, *J. Atmos. Sci., 25*, 323–332, 1968.

Saunders, R. W., L. L. Stowe, G. E. Hunt, and C. F. England, An intercomparison between radiation budget estimates from METEOSAT 1, NIMBUS-7 and TIROS-N satellites, *J. Climate Appl. Meteorol., 22*,546–559, 1983.

Stephens, G. L., G. G. Campbell, and T. H. Vonder Haar, Earth radiation budgets, *J. Geophys. Res., 86*, 9739–9760, 1981.

Stowe, L. L., and M. Fromm, NIMBUS-7 ERB sub-target radiance tape (STRT) data base, *NOAA Tech. Memo NESDIS 3*, 1983.

Stowe, L. L., H. Jacobowitz, and V. R. Taylor, Reflectance characteristics of earth and cloud surfaces as measured by the ERB scanning channels on the NIMBUS 7 satellite, paper pre-

sented at Proceedings International Radiation Symposium, Ft. Collins, Colo., 1980.

Taylor, V. R., and L. L. Stowe, Reflectance characteristics of uniform earth and cloud surfaces derived from NIMBUS 7 ERB, *J. Geophys. Res.*, this issue.

Vonder Haar, T. H., and V. E. Suomi, Measurements of the earth's radiation budget from satellites during a 5-year period, 1, Extended time and space means, *J. Atmos. Sci., 28,* 305–314, 1971.

H. Jacobowitz and L. Stowe, NOAA/National Environmental Satellite Data Information Service, Washington, DC 20233

S. K. Vemury, S M Systems and Research Corporation, Lanham, MD 20706.

(Received March 25, 1983;
revised November 7, 1983;
accepted November 15, 1983.)